Electronic Supplementary Information for

Quasi-2D Co_3O_4 Nanoflakes as Efficient Gas Sensor *versus* Alcohol VOCs

Fedor S. Fedorov,*[a]† Maksim A. Solomatin,[b,c]† Margitta Uhlemann,[d] Steffen Oswald,[d] Dmitry A. Kolosov,[e] Anatolii Morozov,[a] Alexey S. Varezhnikov,[b] Maksim A. Ivanov,[b] Artem K. Grebenko,[a,f] Martin Sommer,[g] Olga E. Glukhova,[e,h] Albert G. Nasibulin,[a,i] and Victor V. Sysoev[b]

[a.] *Skolkovo Institute of Science and Technology, Moscow 121205, Russia.*
[b.] *Yuri Gagarin State Technical University of Saratov, Saratov 410054, Russia.*
[c.] *Saratov Branch of Kotelnikov Institute of Radioengineering and Electronics of RAS, Saratov 410019, Russia.*
[d.] *IFW Dresden, Dresden D-01171, Germany.*
[e.] *Saratov State University, Saratov 410012, Russia.*
[f.] *Moscow Institute of Physics and Technology, Dolgoprudniy 141701, Russia.*
[g.] *Institute for Microstructure Technology, Karlsruhe Institute of Technology (KIT), Eggenstein-Leopoldshafen, Germany.*
[h.] *I.M. Sechenov First Moscow State Medical University, Moscow 119991, Russia.*
[i.] *Aalto University, Aalto 00076, Finland.*
†these authors contributed equally to this work.

Corresponding author: f.fedorov@skoltech.ru

1. Setup applied for deposition of cobalt oxide gas-sensing layer.

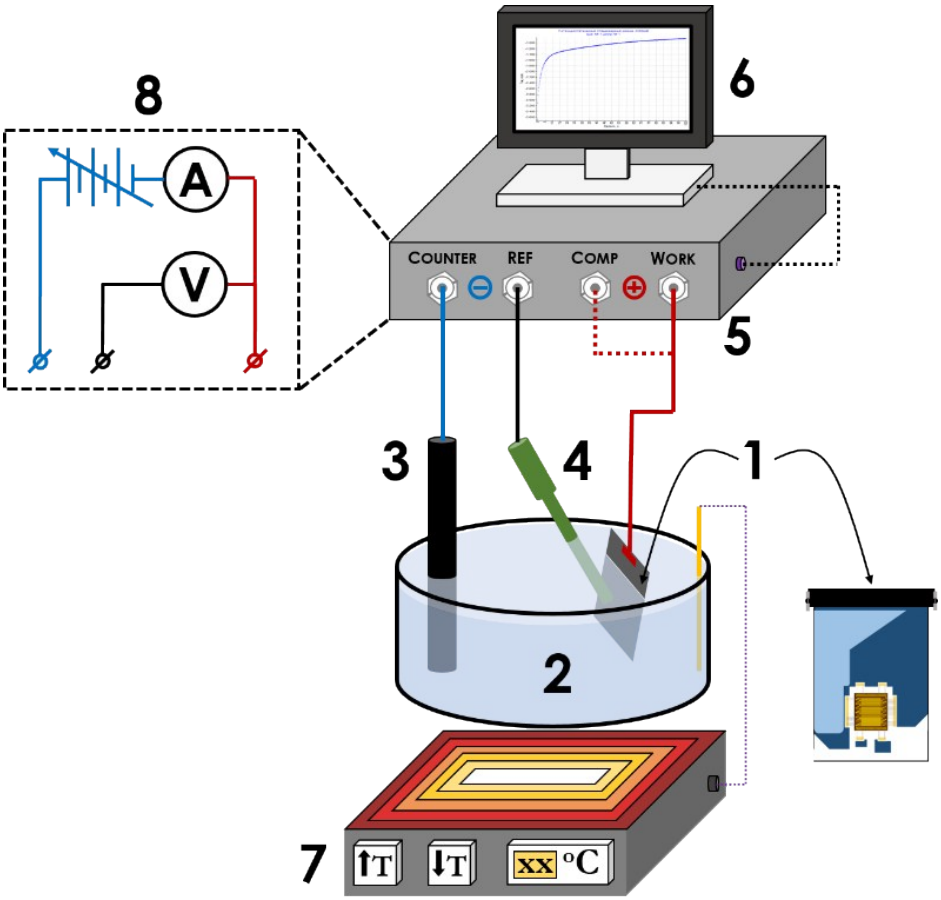

Figure S1. Scheme of the setup used for the deposition of the cobalt oxide layer by electrochemical technique. The numbers indicate: 1 is the multielectroded chip wired at the multi-pin ceramic card (Siegert Co., Switzerland) whose Pt electrodes are employed as a working electrode, 2 is the electrochemical cell filled with the electrolyte, 3 is the graphite counter electrode, 4 is the $Ag/AgCl_{sat.}$ the reference electrode, 5 is the potentiostat, 6 is PC, 7 is a heating plate, 8 is the simplified electrical scheme of measurement in a three-electrode arrangement.

2. Experimental setup to study the chemiresistive response of the Co_3O_4 nanoflaked layer-based gas sensor.

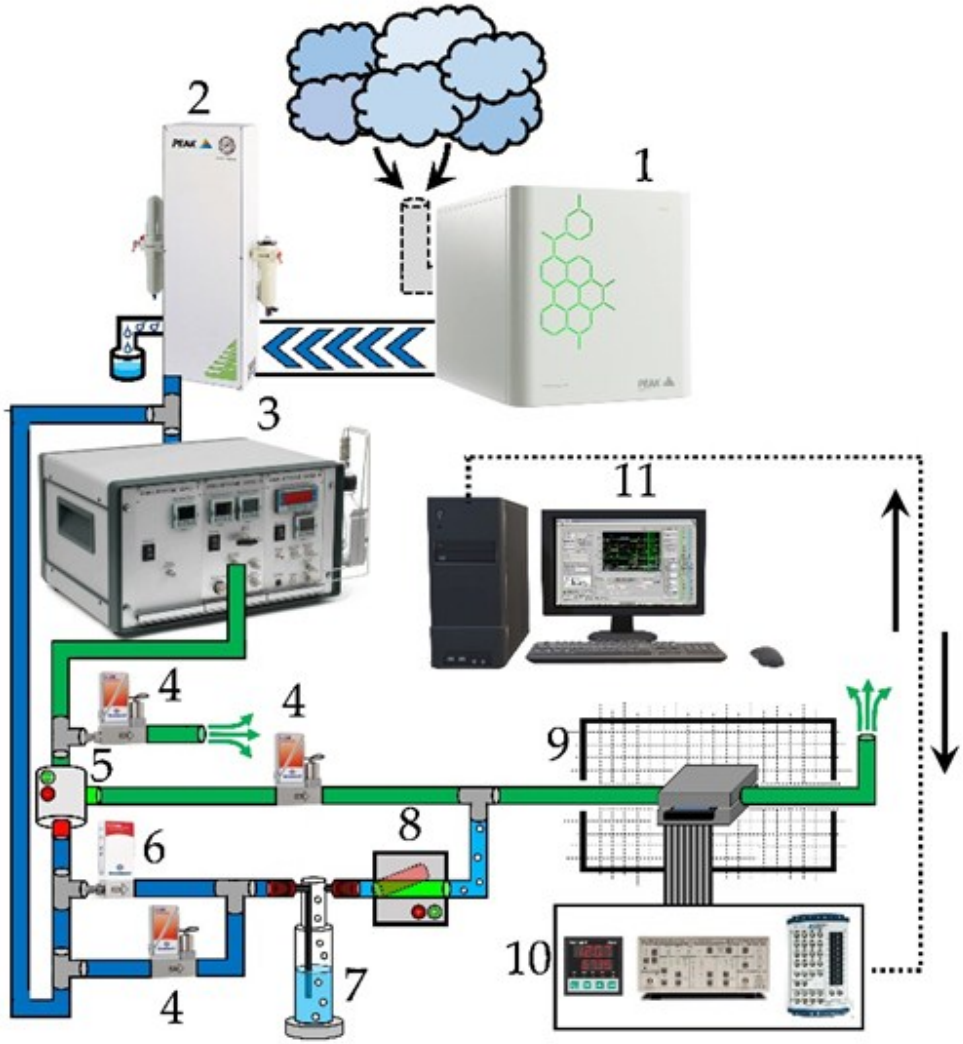

Figure S2. The scheme of the experimental setup to study the chemiresistive response of the Co_3O_4 nanoflaked layer-based gas sensor. The numbers denote: 1 is an air compressor, 2 is a dry air generator (PG14L, Peak Scientific, UK), 3 is a gas generator (OVG-4, Owlstone, UK), 4 is a flow controller, 5 is a switching valve, 6 is a low-flow controller, 7 is a water bubbler, 8 is an opening switch, 9 is the chamber with an installed gas-sensor chip, 10 is the electronic measuring setup, 11 is a PC.

3. Field-effect transistor measurements.

The back gate resistance was measured simultaneously to be always at least two orders larger than the source-drain one. We have tested two similar sensors at room temperature conditions. The samples exhibited relatively a high source-drain resistance of an order of 1 GOhm with a clear response to the back gate voltage illustrated in Figure S3. The observed transconductance behavior depicts *p*-type of major charge carriers in the cobalt oxide layer confirmed by the inclination of this curve showing a greater slope in the region of negative back gate voltages. However, the limitations caused by room temperature conditions and device design do not allow us to calculate mobility and concentration values. The $I_{SD}(V_G)$ curves exhibit a mild hysteresis; the curve's slope does not depend on the source-drain voltage in the measured range of [10:40] V which allows one capturing the source-drain current at nA range.

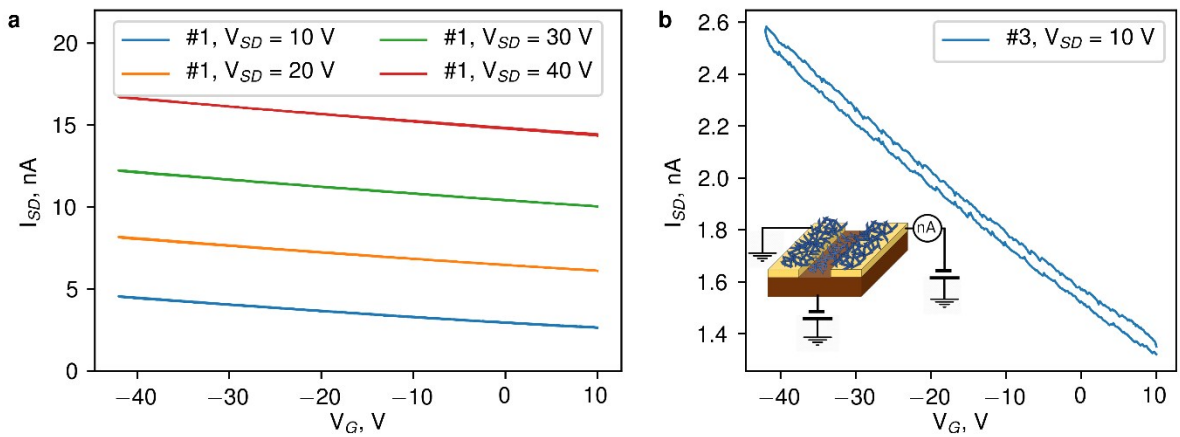

Figure S3. The measurements of cobalt oxide layer transconductance in field-effect transistor (FET) geometry under room temperature. Source-drain current dependence on gate voltage for the sensor element under source-drain voltages to be in the range of [10:40] V (a) and 10 V (b) for sensor elements #1 and #3 correspondingly at the Co_3O_4 nanoflake-based multielectrode chip. Insert at (b) is the cartoon scheme of the measurements.

4. Electrochemical characterization of supporting electrolyte.

Current transient recorded in 0.2 M $NaNO_3$ supporting electrolyte shows an asymptotic decay over time to be linearized at Cottrell coordinates (Figure S1a, inset). The calculated diffusion coefficient seems to be rather small, though this value is effective due to complicated kinetics of the process. Cyclic voltammetry curves are given in Figure S1b to be taken in a few cycles. We can indicate two cathodic processes at -0.25 V and -1.0 V vs. $Ag/AgCl_{sat.}$ correspondingly. The latter process could be also influenced by hydrogen evolution reaction which, in turn, favors a generation of the base.

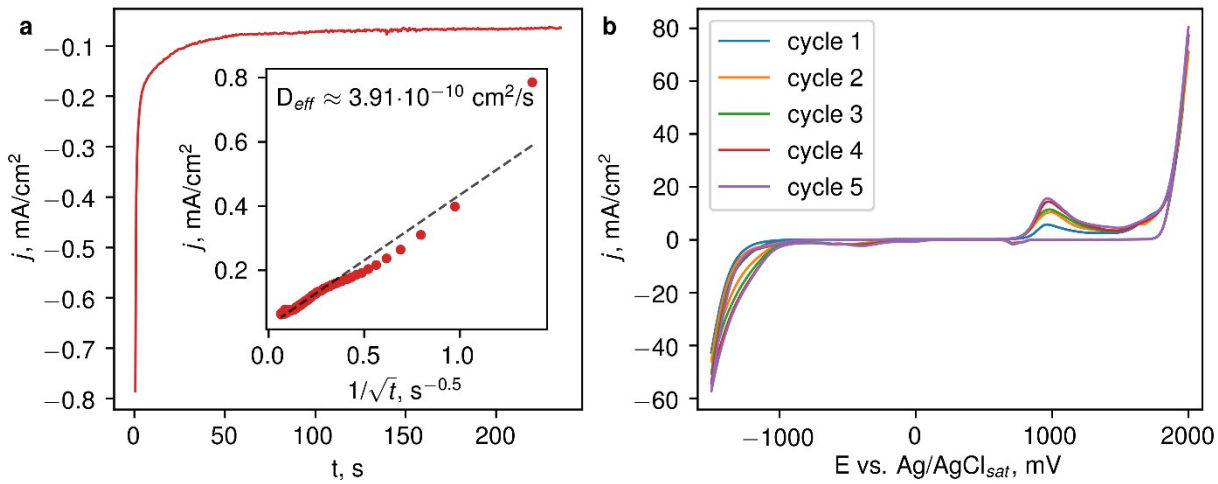

Figure S4. Electrochemical characterization of supporting electrolyte, 0.2 M $NaNO_3$: a) current transient recorded at potential -1V *vs.* $Ag/AgCl_{sat}$; b) cyclic voltammetry results, 5 cycles are presented.

5. TEM characterization of single Co_3O_4 nanoflakes

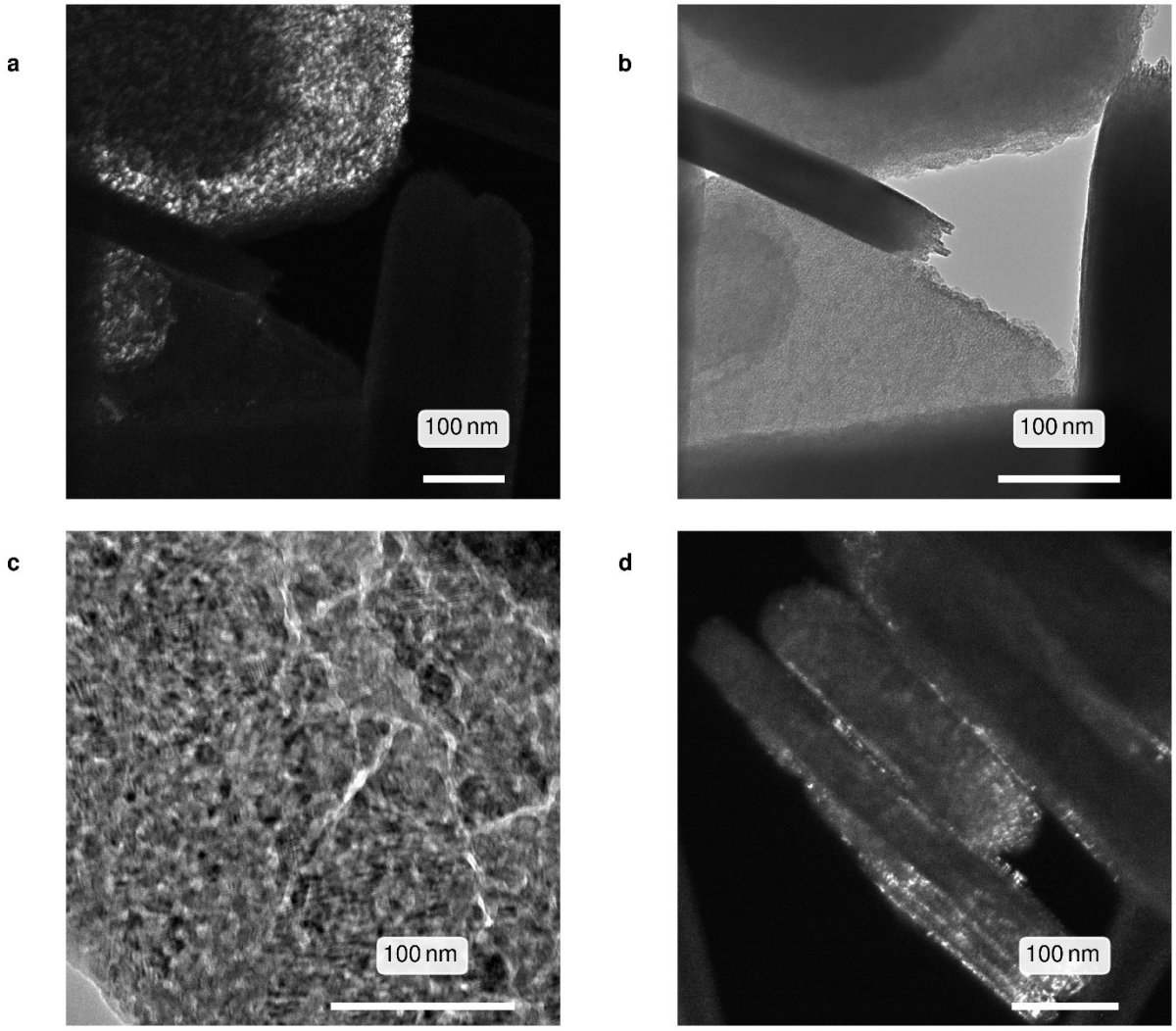

Figure S5. TEM images for as-deposited (cobalt hydroxide) (a,b) and annealed (cobalt oxide) (c,d) samples.

6. XPS deconvolution results for the cobalt oxide layer

We have varied two parameters when we performed annealing of cobalt hydroxide in air, time of treatment and annealing temperature. The evaluated chemical composition is presented in Table S5.

Table S1. XPS results for deconvolution of cobalt core-level spectrum at the as-deposited material

Co2p (As-deposited)									
Band	Pos	PosSep	B_FWHM	FWHM	Height	%Gauss	Area	%Area	ChiSquared
1 - Co2p3/2 peak A	780.50	0.00	2.40	2.40	5885	100	15055	30.29	54.02
2 - Co2p3/2 peak B	782.61	2.11	2.83	2.83	2292	80	7565	15.22	
3- Co2p3/2 satellite	785.90	5.39	5.13	5.13	1652	81	9855	19.83	
4 - Co2p1/2 peak A*	795.98	15.48	3.08	3.08	2100	80	7527	15.15	
5- Co2p1/2 peak B*	797.51	17.00	3.08	3.08	1154	100	3783	7.61	
6 - Co2p1/2 satellite	802.55	22.05	4.72	4.72	1123	90	5913	11.90	

Table S2. XPS results for deconvolution of cobalt core-level spectrum at the material annealed at 300 °C for 4 h

Co2p (Annealed at 300 °C for 4 hours)									
Band	Pos	PosSep	B_FWHM	FWHM	Height	%Gauss	Area	%Area	ChiSquared
1 - Co2p3/2 peak A	780.08	0.00	2.55	2.55	10476	92	29529	45.42	52.74
2 - Co2p3/2 peak B	782.61	2.53	3.08	3.08	3018	100	9894	15.22	
3- Co2p3/2 satellite	788.83	8.75	4.62	4.62	997	100	4905	7.54	
4 - Co2p1/2 peak A*	795.28	15.20	2.64	2.64	4310	80	13288	20.44	
5- Co2p1/2 peak B*	797.51	17.43	2.79	2.79	1367	80	4452	6.85	
6 - Co2p1/2 satellite	804.33	24.25	4.32	4.32	641	100	2943	4.53	

Table S3. XPS results for deconvolution of oxygen core-level spectrum at as-deposited material

O 1s (As-deposited)									
Band	Pos	PosSep	B_FWHM	FWHM	Height	%Gauss	Area	%Area	ChiSquared
1 - low BE	529.93	0.00	2.07	2.07	1256	100	2764	11.31	43.96
2 - higher BE	531.27	1.34	1.90	1.90	10123	88	21686	88.69	

Table S4. XPS results for deconvolution of oxygen core-level spectrum at the material annealed at 300 °C for 4 h

O 1s (Annealed at 300 °C for 4 hours)									
Band	Pos	PosSep	B_FWHM	FWHM	Height	%Gauss	Area	%Area	ChiSquared
1 - low BE	529.63	0.00	1.43	1.43	9468	80	15777	69.50	47.94
2 - higher BE	531.26	1.64	1.90	1.90	3424	100	6925	30.50	

Table S5. The atomic concentration of Co, O, and C estimated out of XPS data for different temperature and time of annealing of the material in comparison with pristine samples

sample	C 1s %	Co 2p %	O 1s %
pristine/as-deposited	8.5	23.1	68.5
25 min. 100°C	40.7	11.3	48.0
50 min. 100°C	39.8	11.2	49.1
250 min. 100°C	37.0	12.1	50.9
25 min. 200°C	32.7	18.7	48.6
50 min. 200°C	33.6	18.0	48.5
250 min. 200°C	31.6	19.9	48.6
25 min. 300°C	31.7	18.2	50.0
50 min. 300°C	31.2	19.1	49.8
250 min. 300°C	27.8	20.0	52.2

7. Study of Co_3O_4 nanoflake layer's impedance at varied a.c. frequencies

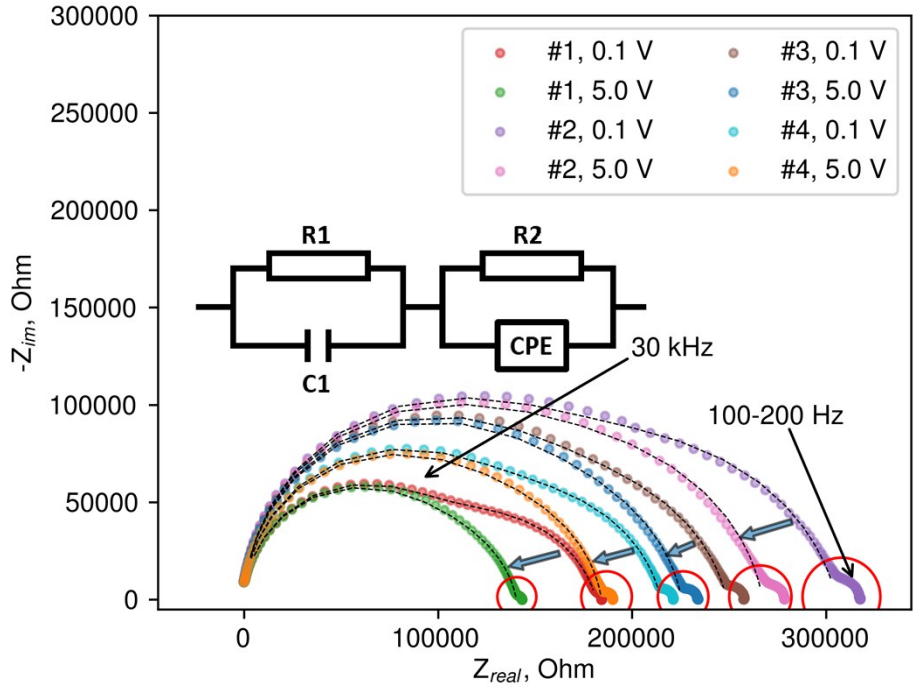

Figure S6. Nyquist plot for three Co_3O_4 nanoflake-based sensors at the multielectrode chip with material deposited for 75 s.

Table S6. Fitted parameters of an equivalent circuit for Co_3O_4 nanoflake-based sensors with material deposited for 75 s.

	R1, Ohm	err, %	C1, F	err, %	R2, Ohm	err, %	CPE-T	err, %	CPE-P	err, %
#1, 0.1 V	92286	1.41	2.37E-11	1.31	89243	1.75	1.49E-09	10.47	0.83	1.34
#1, 5 V	90322	2.56	2.39E-11	2.3	50004	4.62	8.74E-10	20.45	0.87	2.02
#2, 0.1 V	151240	2.4	2.58E-11	2.12	154340	2.53	9.37E-10	14.84	0.84	1.66
#2, 5 V	140770	3.04	2.63E-11	2.51	126530	3.38	5.25E-10	16.33	0.88	1.61
#3, 0.1 V	147400	2.01	2.54E-11	1.74	101270	2.99	1.05E-09	16.07	0.85	1.69
#3, 5 V	143010	2.52	2.57E-11	2.04	82516	4.26	8.24E-10	20.28	0.87	1.85
#4, 0.1 V	119690	1.5	2.60E-11	1.35	95076	2.05	1.02E-09	11.01	0.86	1.28
#4, 5 V	113790	2.64	2.62E-11	2.21	70387	4.26	6.19E-10	18.04	0.89	1.76

8. Estimation of the detection limit for Co_3O_4 nanoflake-based sensor to alcohol VOCs

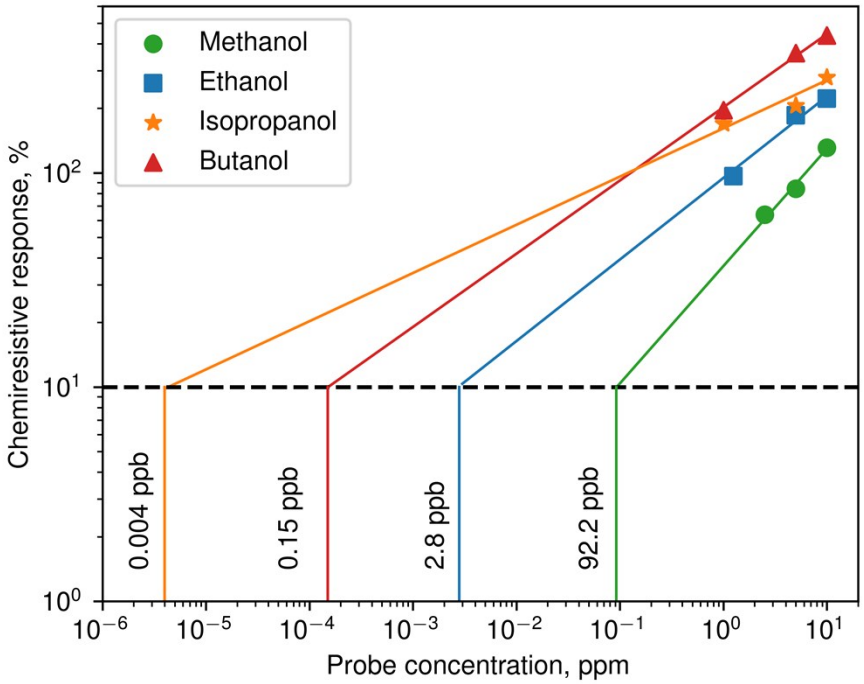

Figure S7. The estimation of the detection limit for Co_3O_4 nanoflake-based sensor to alcohol VOCs, methanol, ethanol, isopropanol, and butanol. The extension follows the empirical Freundlich isotherm.

9. Performance of the same Co_3O_4 nanoflake-based sensor towards butanol with the one-year break at dry and humidified air.

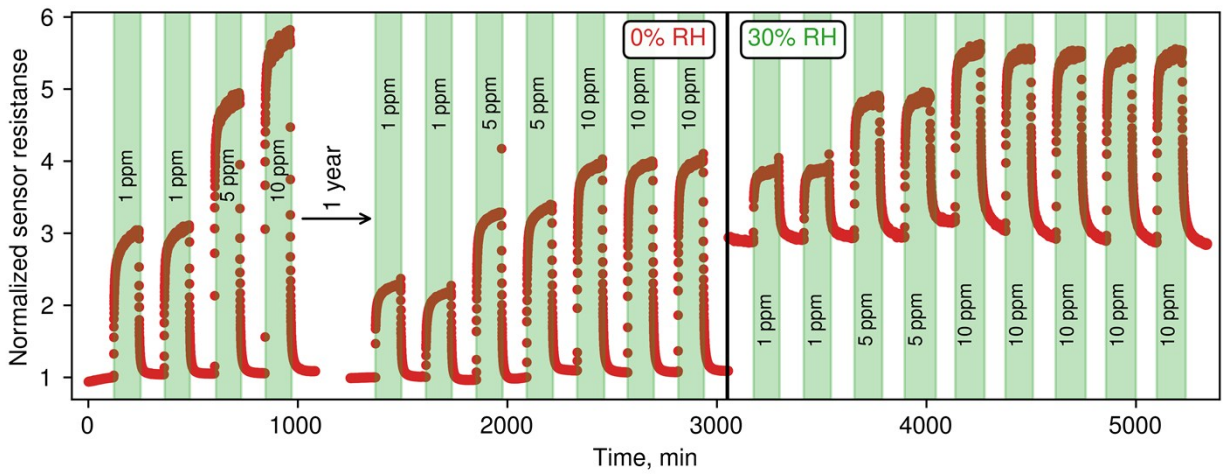

Figure S8. The Co_3O_4-nanoflake based sensor's response to butanol vapors after one year keeping at a shelf in dry air and humid-enriched, 30 rel. %, air.

10. The response of the Co_3O_4 nanoflake-based sensor towards humidity vapors

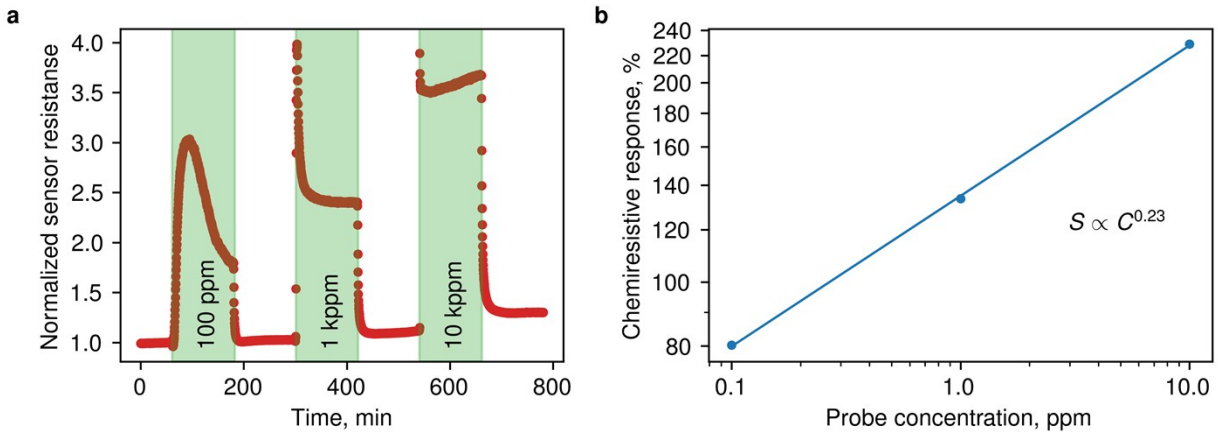

Figure S9. The Co_3O_4-nanoflake based sensor's response to humidity vapors added to air: a) the R(t) transient upon exposure to H_2O vapors, 100-10000 ppm concentrations; b) the dependence of the chemiresistive response on the vapor concentration.

10. Literature review in the field of cobalt oxide gas sensors.

We have reviewed the literature devoted to cobalt oxide-based sensors. The results are presented in Table S7. To properly compare various data, we plot a sensitivity coefficient as a ratio of response in percent to the vapor concentration at *ppm* for methanol, ethanol, isopropanol, and butanol vapors (Figure S10).

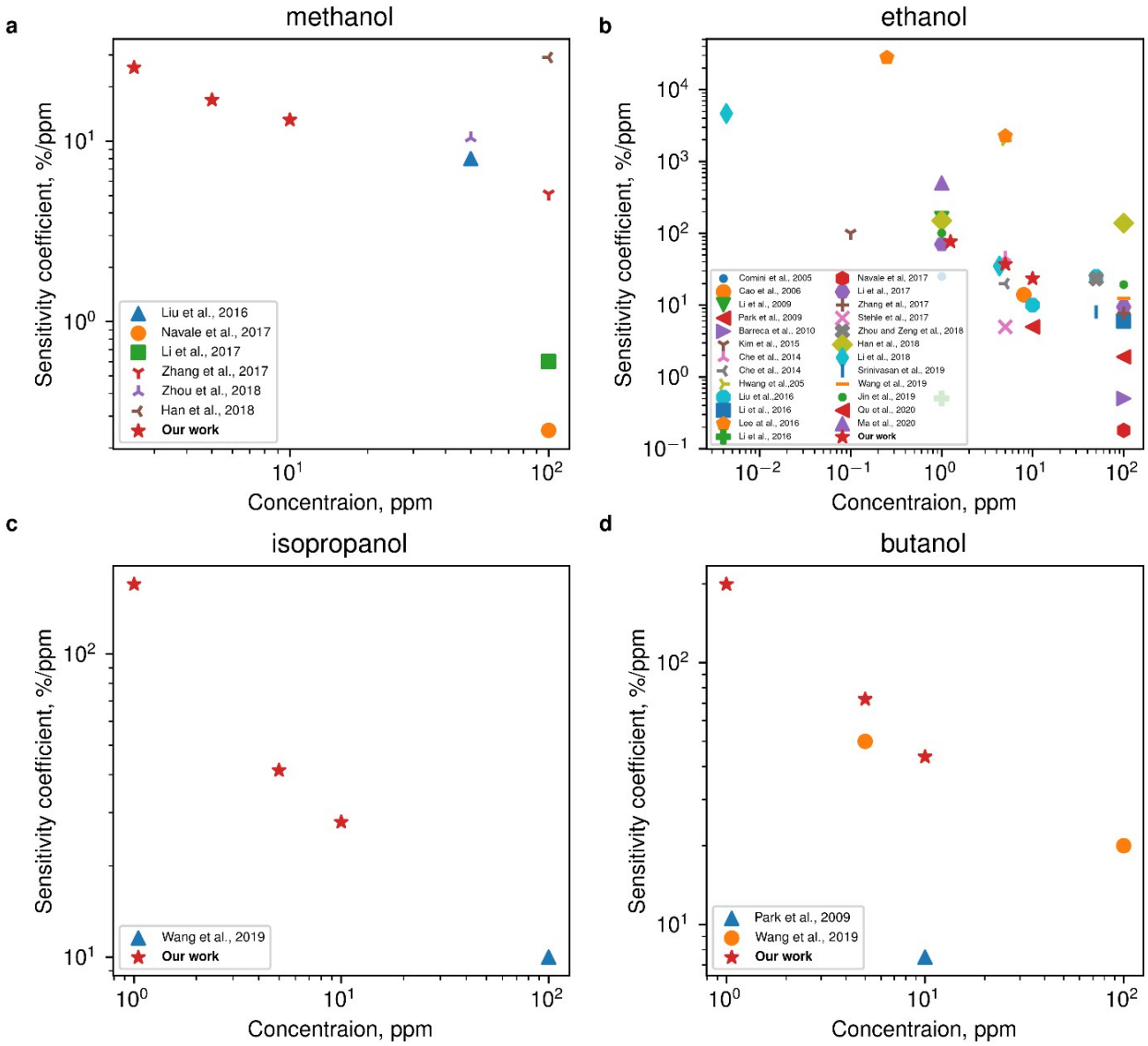

Figure S10. Comparison of sensitivity coefficient of cobalt oxide-based gas sensors upon exposure to methanol (a), ethanol (b), isopropanol (c) and butanol (d).

Table S7. Literature review on cobalt oxide synthesis and sensing performance (analyte, sensitivity, LoD)

Year	Ref.	Method, annealing temperature (°C)	Operation Temperature (optimal), °C	Analyte	Sensitivity calculation method	Sensitivity (min concentration)	Recalculated to $(R_g - R_{air}) \times 100\% / R_{air}$ or $(R_b - R_g) \times 100\% / R_g$, %/ppm	LoD	Notes
2001	s1	Precipitation from cobalt nitrate solution, 800 °C	225	isobutane	$(R_g - R_{air}) \times 100\% / R_{air}$	up to 60%/ 1000 ppm	0.06	n/a	
2003	s2	Reactive electron beam evaporation of cobalt on "pure" and surface-oxidized silicon wafers respectively followed by an additional thermal treatment, 600 °C	240	CH_4	$\Delta R/R_0$	4.5/ 3000 ppm	0.15	n/a	
				H_2		21.7/100 ppm	21.7		
				CO		23.6/ 50 ppm	47.2		
				NO_2		-13.1/ 1 ppm	92.9		
				NH_3		31/ 50 ppm	62		
2005	s3	Reactive radio frequency sputtering	200	NO_2	n/a	26%/200 ppb	n/a	n/a	
			400	acetone		40%/ 20 ppm			
			450	ethanol		25%/1 ppm			
			400	benzene		22%/ 5 ppm			
			400	ethyl acetate		9%/ 1 ppm			
			400	CO		the lowest concentration reported - 10 ppm			
2006	s4	n/a, possibly co-precipitation and hydrothermal methods	80	CO	R_g/R_a	3.8/1000 ppm	0.28	n/a	

		using cobalt nitrate precursor	100	H_2		3/ 1000 ppm	0.2		
			90	CH_4		1.3/ 1000 ppm	0.3		
2006	s5	Two-step method: cobalt acetate reacts with ethylene glycol (EG) in the presence of poly(vinyl pyrrolidone) (PVP) to produce cobalt oxide precursor, and then the precursor is calcinated to produce Co_3O_4, 500 °C	300	CO	R_g/R_a	ca. 1.9/1000 ppm	0.0009	n/a	
				ethanol		>8/50 ppm	14		
2009	s6	Obtained at 300 °C from the $CoCO_3$ submicrometer crystals after thermal transformation in laboratory air	300	ethanol	R_g/R_a	ca. 2.6/1 ppm	160	n/a	
				CO		ca. 1.4/10 ppb	4000		
2009	s7	Template replication method and immobilization using dielectrophoresis process, using SBA-15, cobalt nitrate, 450 °C	200	CO	$(R_g - R_{air}) \times 100\%/ R_{air}$	4.3%/10 ppm	0.43	n/a	
2009	s8	Pulsed laser deposition	400	CO	R/R_0	ca. 1.2/20 ppm	1	n/a	
				NO_2		ca. 0.9/5 ppm	2.2		
				CH_4		ca. 1.05/20 ppm	0.25		
2009	s9	Hydrothermal, using SBA-15, SBA-40b, SBA-100b and cobalt	200	CO	$[(R_g - R_{air})/R_{air}] \times 100\%$	ca. 10%/ 10 ppm	1	n/a	

		nitrate							
2009	s10	Surfactant-assisted (SDBS) solvothermal method	100	toluene	R_g/R_a	3.1/ 10 ppm	21	n/a	
				acetone		ca. 2.6/ 10 ppm	16		
				ethanol		ca. 1.5/ 10 ppm	5		
				gasoline		ca.1.8/ 10 ppm	8		
				propanol		ca. 1.75/ 10 ppm	7.5		
				butanol		ca. 1.75/ 10 ppm	7.5		
2010	s11	Chemical Vapor Deposition route under O_2 + H_2O atmospheres at 500 °C.	200	ethanol	relative resistance variation upon exposure to the target gases	ca. 0.5/100 ppm	0.5	n/a	
				H_2		ca. 0.6/1000 ppm	0.6		
2012	s12	Modified template 2 step method, using SBA-15 and cobalt nitrate	350	ethanol		5.1/300 ppm	n/a	n/a	
2014	s13	Thermal decomposition of cobalt nitrate at ZnO-PVP (250, 350 °C) followed by etching of ZnO.	220	HCOH	R_g/R_a	1.05/50 ppb	100	5 ppb/ 50 ppb	
				NO_2		ca. 1.02/100 ppb	20		
				CO		ca. 1.03/100 ppb	30		
				CO_2		ca. 1.01/100 ppm	0.01		
				ethanol		1.1/100 ppb	100		
2014	s14	Synthesized by sacrificial CNTs through SPMIC method using	300	acetone	R_g/R_a	low		n/a	

		$Co(NO_3)_2$ precursor, 650 °C		toluene		low			
				formaldehyde		low			
				ammonia		1.1/ 10 ppm	1		
2014	s15	Synthesized via a facile template-free hydrothermal method and subsequent thermal decomposition	200	ethanol	R_g/R_a	ca. 3.3/ 5 ppm	46	n/a	
2014	s16	Ethylene glycol (EG)-mediated solvothermal method followed by calcination	180	ethanol	R_g/R_a	2/5 ppm	20	n/a	
2014	s17	Fluoride anion-assisted hydrothermal and controlled annealing route, 350 °C	100	H_2	R_g/R_a	1.05/10 ppm	0.5	n/a	F-doped
				CO		ca. 3.5/10 ppm	25		
2015	s18	Thermal decomposition of cobalt nitrate by nanocasting, using KIT-6 silica as a structure matrix with further removal of silica matrix by sodium hydroxide, 300 °C	200	CO	R_g/R_a	ca. 1.2/1 ppm	20	n/a	
2015	s19	Purchased or prepared by the solvothermal reaction of stock solutions and subsequent heat treatment (powders, hollow spheres, hollow hierarchical nanostructures), 400 °C	250	p-xylene	R_g/R_a	ca. 170/5 ppm	3380	n/a	in comparison with Pt-modified hierarchical cobalt oxide nanostructures
				ethanol		ca. 100/5 ppm	1980		
				p-xylene (275)		ca. 100/ 5 ppm	1980		
				toluene (275)		ca. 70/5 ppm	1380		
				formaldehyde (275)		ca. 10/5 ppm	180		

				benzene (275)		ca. 7/5 ppm	120		
				ethanol (275)		ca. 21/5 ppm	400		
				ammonia (275)		ca. 4/5 ppm	60		
				hydrogen (275)		ca. 1/5 ppm	-		
2016	s20	Commercial powder. A ceramic paste of the sensing material powder was prepared by mixing an organic dispersant consisting of 10 wt % ethyl cellulose and 90 wt % terpineol. The weight ratio of the sensing material powder to the organic dispersant was 1:16. The sensor was baked at 400 °C	100 200	NO	R_g/R_a	1.11/ 50 ppb	220	n/a	in comparison with Ag, Au, Pt modified powders
				H_2		1.27/ 25 ppm	1.08		
2016	s21	Solvothermal process using poly(vinylpyrrolidone) to control morphology, 500 °C	170	ethanol	R_g/R_a	2/10 ppm (13.4/ 50 ppm)	10 (25)	n/a	
				xylene		ca. 1.1/ 50 ppm	0.2		
				ether		ca. 2/ 50 ppm	2		
				acetone		ca. 6/ 50 ppm	10		
				methanol		ca. 5/ 50 ppm	8		
				ethylbenzene		ca. 2/ 50 ppm	2		
				toluene		ca. 1.5/ 50 ppm	1		
				benzene		ca. 1/ 50 ppm	-		

2016	s22	Nanocasting method with ordered mesoporous silica as a hard template (KIT-6, SBA-15), $Co(NO_3)_2 \cdot 6H_2O$, 400 °C	175-200	ethanol	R_g/R_a or R_a/R_g	7/ 100 ppm (concentration dependence is not discussed and hard to consider)	6	n/a	
				NO_2		ca. 1.5/100 ppm	0.5		
				H_2		- (ca. 1/100 ppm)	-		
				formaldehyde		ca. 2.5/100 ppm	1.5		
				acetone		ca. 2.9/100 ppm	1.9		
				toluene		ca. 2.4/100 ppm	1.4		
				methane		ca. 2/ 100 ppm	1		
2016	s23	Transferring cobalt-solution-dipped polystyrene mono-layers onto sensor substrates and subsequent removal of the PS template by heat treatment, 400 °C	200 250 275	ethanol	$(R_g-R_a)/R_a$	112.9/5 ppm, ca. 70/0.25 ppm	2258, 28000	sub-ppb	the exact value of LoD for ethanol is not indicated
				xylene		ca. 20.7/5 ppm, 1/0.25 ppm	414, 400	0.05 ppm	
				toluene (200)		ca. 37/5 ppm	740		
				benzene (200)		ca.25/5 ppm	500		
				HCHO (200)		ca. 5/5 ppm	100		
				CO (200)		ca. 4/5 ppm	80		
2016	s24	Hydrothermal route using cobalt nitrate and NH_4F, 350 °C	RT	NH_3	R_g/R_a	ca. 1.2/0.2 ppm, 9.5/100 ppm	100, 8.5	0.2 ppm	
				H_2S		2.0/100 ppm	1		
				CO		1.4/100 ppm	0.4		

				H_2		1.2/100 ppm	0.2		
				C_2H_5OH		1.5/100 ppm	0.5		
2017	s25	Chemical bath deposition, cobalt nitrate, urea, and ammonium fluoride. 400 °C	200	NO_2	$(R_g - R_{air}) \times 100\% / R_{air}$	16%/100 ppm	0.16	n/a	
				Cl_2		22%/100 ppm	0.22		
				H_2S		340%/100 ppm, 68%/5 ppm	3.4, 13.6		
				NH_3		46%/100 ppm	0.46		
				CH_3OH		25%/100 ppm	0.25		
				C_2H_5OH		18%/100 ppm	0.18		
2017	s26	Hydrothermal treatment and a post thermal annealing procedure of cobalt nitrate at carbon foam, 200, 250 and 350 °C	100	ethanol	R_g/R_a	ca. 1.7/1 ppm, 10.4/ ~100 ppm	70, 9.4	0.2 ppm	
				toluene		ca. 1.1/ ~100 ppm	0.1		
				NO_2		ca. 0.9/ about 10 ppm	-1		
				NH_3		ca. 1.05/ ~100 ppm	0.05		
				methanol		ca. 1.6/ ~100 ppm	0.6		
				formaldehyde		ca. 1.5/ ~100 ppm	0.5		
				ethylene glycol		ca. 4.9/ ~100 ppm	3.9		
				CO		ca. 1.06/ about 10 ppm	0.6		
				benzyl alcohol		ca. 2.3/ ~100 ppm	1.3		
				acetone		ca. 1.25/ ~100 ppm	0.25		
2017	s27	Post-thermal conversion of $(Co(NH_3)_6)CoF_6 \cdot H_2O$ precursor	111	acetone	R_g/R_a	6.8/20 ppm, 16.5/ 100	29, 15.5	n/a	

		after a fluorine-assisted hydrothermal route, 350 °C				ppm			
				pentane		4.8/100 ppm	3.8		
				ammonia		5.6/100 ppm	4.6		
				methanol		6.1/100 ppm	5.1		
				formaldehyde		6.4/100 ppm	5.4		
				ethanol		8.7/100 ppm	7.7		
2017	s28	Precipitation and subsequent thermal decomposition of a carbonate precursor, 500 °C	120	CO	R_{CO}/R_{air}	ca. 5.1/6.7 ppm	61.2	n/a	different humidity
			240			ca. 2.4/6.7 ppm	20.9		
2017	s29	Solution-combustion synthesis, 350°C (and annealing at 300 or 600 °C)	100 (25% RH) 150 (dry air)	acetone	R_g/R_a	6.3/10 ppm (150 °C in humid air)	53	n/a	
				ethane		3.7/250 ppm (125 °C in dry air)	1.08		
				CO		3.6/100 ppm (100 °C in dry air)	2.6		
2017	s30	Atomic layer deposition	350	ethanol	I_{air}/I_{gas}	ca. 1.25/5 ppm	5	n/a	
2018	s31	Hydrothermal method using cobalt nitrate precursor, 500 °C	200	ethanol	R_g/R_a	12.6/50 ppm	23.2	n/a	
				methanol		ca. 6.2/50 ppm	10.4		
				ammonia		ca. 4.3/50 ppm	6.6		
				acetone		ca. 8.2/50 ppm	14.4		
2018	s32	Hydrothermal method, 300-500 °C	185	ethanol	R_g/R_a	2.5/1 ppm, ca. 140/100 ppm	150, 139	n/a	
				acetone		ca. 60/ 100 ppm	59		

				methanol		ca. 30/100 ppm	29		
				formaldehyde		ca. 55/100 ppm	54		
				ammonia		ca. 29/100 ppm	28		
				nitrogen dioxide		ca.2/100 ppm	1		
2018	s33	Synthesized using cobalt nitrate precursor at polystyrene spheres and 2-methylimidazole. The templates are removed using the organic solvent methylbenzene, 300-450 °C.	200	ethanol	R_g/R_a	ca. 1.2/4.3 ppb, ca. 2.5/4.3 ppm	4651.2, 34.9	4.3 ppb	
				H_2S		ca. 1.3/4.3 ppm	7.0		
				NH_3		ca. 1.25/4.3 ppm	5.8		
				CH_3OCH_3		ca. 2.0/4.3 ppm	23.3		
				HCHO		ca. 1.26/4.3 ppm	6.0		
				NO_2		1.25/4.3 ppm	5.8		
			170	C_2H_6S		ca. 1.3/250 ppb, 3.15/125 ppm	120, 1.72		
				CH_4S		ca. 1.7/125 ppm	0.6		
				CH_3COCH_3		ca. 2.1/125 ppm	0.9		
				H_2S		ca. 1.45/125 ppm	0.36		
				HCHO		ca. 1.5/125 ppm	0.4		
				NH_3		ca. 1.7/125 ppm	0.6		
2019	s34	Oxygen plasma treatment of a metal containing polymer (PVA) film followed by heat treatment, 500 °C.	200	formaldehyde	$(R_g - R_{air}) \times 100\% / R_{air}$	5%/50 ppb	100	40 ppb	
				H_2		ca. 12%/500 ppm	0.024		
				NH_3		ca. 2.5%/1 ppm	2.5		

				CO_2		-	-		
2019	s35	Spray pyrolysis (cobalt acetate tetrahydrate) technique at different deposition temperatures, 473 to 773 K in steps of 100 K	RT	acetone	$R_{analyte}/R_{air}$	235/50 ppm	468	1 ppm	
				ethanol		ca. 5/50 ppm	8		
				ammonia		ca. 4/50 ppm	6		
				xylene		ca. 1/50 ppm	-		
				toluene		ca. 2/50 ppm	2		
				acetaldehyde		ca. 30/50 ppm	58		
2019	s36	Porous Co_3O_4 assembled from nanoparticles was acquired by heating Co-MOFs which were prepared using Co^{2+} ions and 2-methylimidazole at room temperature	100	n-butanol	R_g/R_a	21/100 ppm, ca. 3.5/5 ppm	20, 50	n/a	
				butanone		ca. 12.5/100 ppm	11.5		
				isopropanol		ca.11/100 ppm	10		
				xylene		ca. 7.5/100 ppm	6.5		
				ammonia		ca. 2.4/100 ppm	1.4		
				methylbenzene		ca. 6.2/100 ppm	5.2		
				acetone		ca. 5.2/100 ppm	4.2		
				ethanol		ca. 13.5/100 ppm	12.5		
2019	s37	Sol–gel, using precursor $Co(CH_3COO)_2.4H_2O$, 600 °C	n/a	LPG	R_g/R_a	ca. 1.15/1000 ppm	0.015	n/a	
2019	s38	Wet-chemical method, cobalt acetate, urea. 300 °C	300	ethanol	R_g/R_a	ca. 2/1 ppm, 20.3/100 ppm	100, 19.3	1 ppm	
				formaldehyde		3.2/100 ppm	2.2		

				acetone		4.8/100 ppm	3.8		
				methane		1.4/100 ppm	0.4		
				benzene		2.1/100 ppm	1.1		
				ammonia		2.5/100 ppm	1.5		
2020	s39	Electrospinning method using ethanol or N,N-dimethylformamide (DMF) solvents mixed with cobalt(II) nitrate and polyvinylpyrrolidone (PVP) applied for the electrospinning, 600 °C.	100	CO	R/R_0, R_0/R	2.4/5 ppm	28		
				NO_2		ca. -0.8/5 ppm	n/d		
				C_2H_6O		ca. 0.5/5 ppm	n/d		
				H_2		ca. 0.1/5 ppm	n/d		
2020	s40	Co_3O_4 microspheres are synthesized via amorphous-coordination polymers based self-template method, 500 °C.	220	xylene	R_g/R_a	ca. 3/10 ppm	20	0.35 ppm	
				toluene		ca. 2.9/100 ppm	1.9		
				benzene		ca. 1.5/100 ppm	0.5		
				acetone		ca. 3/100 ppm	2		
				ethanol		ca.2.9/100 ppm	1.9		
				formaldehyde		ca.2.8/100 ppm	1.8		
2020	s41	Combination of an h-CoO → β-$Co(OH)_2$ phase transition followed by thermal oxidation led to the spontaneous deposition of Co_3O_4 on interdigitated electrodes, 500 °C.	200	acetone	R_g/R_a, R_a/R_g	ca. 1.07/20 ppb, 12.4/1 ppm	350, 1240	13.8 ppb	
				ethanol		ca. 6/1 ppm	500		
				C_6H_6		ca. 5/1 ppm	400		
				CH_2O		ca. 3/1 ppm	200		

				NH_3		ca. 2/1 ppm	100		
				NO_2		ca. 2.1/1 ppm	1.1		
2020	s42	Polyol approach using cobalt (II) acetylacetonate precursor and PVP, 500 °C	170	CO	I_g/I_a	1.57/300 ppm	n/a	n/a	

There are several reviews on Co_3O_4, i.e. by J.M. Xu and J.P. Cheng [43] and by X. Wang et al. [44]

References:

s1 S.-D. Choi and B.-K. Min, Sensors Actuators B Chem., 2001, 77, 330–334.

s2 J. Wöllenstein, M. Burgmair, G. Plescher, T. Sulima, J. Hildenbrand, H. Böttner and I. Eisele, Sensors Actuators B Chem., 2003, 93, 442–448.

s3 E. Comini, G. Faglia, M. Ferroni, G. Sberveglieri and M. Sacerdoti, in SENSORS, 2005 IEEE, 2005, pp. 1323-1325.

s4 R.-J. Wu, J.-G. Wu, T.-K. Tsai and C.-T. Yeh, Sensors Actuators B Chem., 2006, 120, 104–109.

s5 A.-M. Cao, J.-S. Hu, H.-P. Liang, W.-G. Song, L.-J. Wan, X.-L. He, X.-G. Gao and S.-H. Xia, J. Phys. Chem. B, 2006, 110, 15858–15863.

s6 C. C. Li, X. M. Yin, T. H. Wang and H. C. Zeng, Chem. Mater., 2009, 21, 4984–4992.

s7 C.-Y. Liu, C.-F. Chen and J.-P. Leu, Electrochem. Solid-State Lett., 2009, 12, J40.

s8 I. Kärkkänen, A. Floren, H. Mändar, T. Avarmaa and R. Jaaniso, Procedia Chem., 2009, 1, 654–657.

s9 C.-Y. Liu, C.-F. Chen and J.-P. Leu, Sensors Actuators B Chem., 2009, 137, 700–703.

s10 J. Park, X. Shen and G. Wang, Sensors Actuators B Chem., 2009, 136, 494–498.

s11 D. Barreca, E. Comini, A. Gasparotto, C. Maccato, A. Pozza, C. Sada, G. Sberveglieri and E. Tondello, J. Nanosci. Nanotechnol., 2010, 10,

8054–8061.

s12 M. Ma, Z. Pan, L. Guo, J. Li, Z. Wu and S. Yang, Chinese Sci. Bull., 2012, 57, 4019–4023.

s13 J. Y. Kim, N.-J. Choi, H. J. Park, J. Kim, D.-S. Lee and H. Song, J. Phys. Chem. C, 2014, 118, 25994–26002.

s14 S. Yi, S. Tian, D. Zeng, K. Xu, X. Peng, H. Wang, S. Zhang and C. Xie, Sensors Actuators B Chem., 2014, 204, 351–359.

s15 H. Che, A. Liu, J. Hou, X. Zhang, Y. Bai, J. Mu and R. Wang, Mater. Res. Bull., 2014, 59, 69–76.

s16 H. Che, A. Liu, X. Zhang, J. Hou, J. Mu and H. He, Nano, 2014, 09, 1450071.

s17 Z. Dou, C. Cao, Y. Chen and W. Song, Chem. Commun., 2014, 50, 14889–14891.

s18 S. Vetter, S. Haffer, T. Wagner and M. Tiemann, Sensors Actuators B Chem., 2015, 206, 133–138.

s19 S.-J. Hwang, K.-I. Choi, J.-W. Yoon, Y. C. Kang and J.-H. Lee, Chem. – A Eur. J., 2015, 21, 5872–5878.

s20 T. Akamatsu, T. Itoh, N. Izu and W. Shin, Sensors Mater., 2016, 28, 1191–1201.

s21 T. Liu, J. Liu, Q. Liu, Y. Sun, X. Jing, H. Zhang and J. Wang, CrystEngComm, 2016, 18, 5728–5735.

s22 Q. Li, Y. Du, X. Li, G. Lu, W. Wang, Y. Geng, Z. Liang and X. Tian, Sensors Actuators B Chem., 2016, 235, 39–45.

s23 C.-S. Lee, Z. Dai, S.-Y. Jeong, C.-H. Kwak, B.-Y. Kim, D. H. Kim, H. W. Jang, J.-S. Park and J.-H. Lee, Chem. – A Eur. J., 2016, 22, 7102–7107.

s24 Z. Li, Z. Lin, N. Wang, J. Wang, W. Liu, K. Sun, Y. Q. Fu and Z. Wang, Sensors Actuators B Chem., 2016, 235, 222–231.

s25 S. T. Navale, C. Liu, P. S. Gaikar, V. B. Patil, R. U. R. Sagar, B. Du, R. S. Mane and F. J. Stadler, Sensors Actuators B Chem., 2017, 245, 524–532.

s26 L. Li, C. Zhang, R. Zhang, X. Gao, S. He, M. Liu, X. Li and W. Chen, Sensors Actuators B Chem., 2017, 244, 664–672.

s27 Z. Zhang, L. Zhu, Z. Wen and Z. Ye, Sensors Actuators B Chem., 2017, 238, 1052–1059.

s28 S. Vladimirova, V. Krivetskiy, M. Rumyantseva, A. Gaskov, N. Mordvinova, O. Lebedev, M. Martyshov and P. Forsh, Sensors (Switzerland), 2017, 17, 2216.

s29 K. Vojisavljević, S. Wicker, I. Can, A. Benčan, N. Barsan and B. Malič, Adv. Powder Technol., 2017, 28, 1118–1128.

s30 J. Stehle, A. K. Samarao, U. Krishnamoorthy and O. Ambacher, in TRANSDUCERS 2017 - 19th International Conference on Solid-State Sensors, Actuators and Microsystems, 2017, pp. 1504–1507.

s31 Q. Zhou and W. Zeng, Phys. E Low-dimensional Syst. Nanostructures, 2018, 95, 121–124.

s32 D. Han, Y. Ji, F. Gu and Z. Wang, J. Colloid Interface Sci., 2018, 531, 320–330.

s33 Y. Li, F. Zhou, L. Gao and G. Duan, Sensors Actuators B Chem., 2018, 261, 553–565.

s34 H. Long, S. Turner, A. Yan, H. Xu, M. Jang, C. Carraro, R. Maboudian and A. Zettl, Sensors Actuators B Chem., 2019, 301, 127067.

s35 P. Srinivasan, A. J. Kulandaisamy, G. K. Mani, K. J. Babu, K. Tsuchiya and J. B. B. Rayappan, RSC Adv., 2019, 9, 30226–30239.

s36 M. Wang, Z. Shen, X. Zhao, F. Duanmu, H. Yu and H. Ji, J. Hazard. Mater., 2019, 371, 352–361.

s37 P. K. Singh, N. Singh, M. Singh, P. Tandon and S. K. Singh, J. Mater. Eng. Perform., 2019, 28, 7592–7601.

s38 Z. Jin, L.-P. Wang, Y. Zhang, J. Fan, M.-H. Liao, X.-F. Wang and Y. Ding, J. Nanoparticle Res., 2019, 21, 115.

s39 C. Busacca, A. Donato, M. Lo Faro, A. Malara, G. Neri and S. Trocino, Sensors Actuators B Chem., 2020, 303, 127193.

s40 F. Qu, N. Zhang, D. Liu, S. Zhang, B. Talluri, Y. Zheng, T. Thomas, R. Zhao, S. Ruan and M. Yang, Sensors Actuators B Chem., 2020, 308, 127651.

s41 A. Ma, H. J. Park, J. H. Seo, K. Y. Jang, H. K. Lee, D. Y. Kim, J. E. Lee, K. M. Nam and D.-S. Lee, Sensors Actuators B Chem., 2020, 308, 127698.

s42 K.-W. Chen, J.-H. Tsai and C.-H. Chen, J. Alloys Compd., 2020, 816, 152524.

s43 J. M. Xu and J. P. Cheng, J. Alloys Compd., 2016, 686, 753–768.

s44 X. Wang, W. Tian, T. Zhai, C. Zhi, Y. Bando and D. Golberg, J. Mater. Chem., 2012, 22, 23310–23326.